

This copy is for your personal, non-commercial use only.

If you wish to distribute this article to others, you can order high-quality copies for your colleagues, clients, or customers by [clicking here](#).

Permission to republish or repurpose articles or portions of articles can be obtained by following the guidelines [here](#).

The following resources related to this article are available online at www.sciencemag.org (this information is current as of April 7, 2010):

Updated information and services, including high-resolution figures, can be found in the online version of this article at:

<http://www.sciencemag.org/cgi/content/full/327/5969/1119>

Supporting Online Material can be found at:

<http://www.sciencemag.org/cgi/content/full/science.1182781/DC1>

A list of selected additional articles on the Science Web sites **related to this article** can be found at:

<http://www.sciencemag.org/cgi/content/full/327/5969/1119#related-content>

This article **cites 20 articles**, 13 of which can be accessed for free:

<http://www.sciencemag.org/cgi/content/full/327/5969/1119#otherarticles>

This article has been **cited by** 1 articles hosted by HighWire Press; see:

<http://www.sciencemag.org/cgi/content/full/327/5969/1119#otherarticles>

This article appears in the following **subject collections**:

Geochemistry, Geophysics

http://www.sciencemag.org/cgi/collection/geochem_phys

Table 1. Bidart Fan earthquake sequence, channel incision, and offset events.

Earthquake date*	Inferred incision date	Channel	Total offset (m)	Number of offsets
(A) 1857			5.9	
(B) 1631–1823				
(C) 1547–1617§	1605 ± 5	SE	10.2†	25
(D) ~1450–1547‡				
(E) ~1450–1547‡				
(F) 1360–1425#	1418 ± 10	NW	15.9†	5
(G) 1280–1340				

*Dates from (15) except as noted. Earthquake F is rupture event BDT4-d at trench T4. Earthquake G is rupture BDT4-e at T4. Earthquakes BDT3-f and BDT3-g at T3 (15) are older than earthquakes F and G in this table. †Measurements from (8). ‡Approximate age (21). §Inferred incision age of southeast channel overlaps with dates of second and third earthquakes reported by Akçiz *et al.* (15). They presented evidence that event BDT2-b is the third oldest earthquake, event C, and predates incision. New radiocarbon dates of BDT2-b (17) eliminate age overlap of earthquakes B and C. #The sixth earthquake, F, caused surface rupture between deposition of two near-surface sedimentary units (17) and therefore is inferred to predate incision of the adjacent northwest channel.

same-age sediments in trenches ~200 m away suggests that the northwest channel has been displaced by five surface ruptures (Table 1). Ages of sediments and their stratigraphic position in trench 4 support an interpretation of incision between the fifth and sixth earthquakes, during a time interval that includes the ~1418 extreme flood (17) (Table 1). Thus, the northwest channel has been offset in three additional earthquakes by as much as 5.6 m more than the offset of the southeast channel (Fig. 2). Slip in individual earthquakes at the BF is not directly measurable, but we can assume at least 50 cm of slip on the basis of expression in trench exposures (15). With minimum slip of 1 m in two earthquakes, maximum slip would be 4.6 m in the other earthquake.

Comparison of channel incision dates with the rate of occurrence of surface ruptures suggests that channel incision events are less frequent than earthquakes in the Carrizo Plain, which implies

that some channels have been offset by more earthquakes than previously thought (9). Our observations do not support previous interpretations of ~9 m of slip in the 1857 earthquake (3, 4) or any of the earthquakes that ruptured since 1400. However, slip in the 1857 earthquake was apparently greater than in any of the four prior ruptures. This variable slip history is not consistent with repeated characteristic slip (20) at BF in the Carrizo, one of two areas where characteristic slip was defined (6). Since the 1857 earthquake, >5 m of strain has accumulated in the Carrizo, an amount greater than or similar to slip released in the last five ruptures.

References and Notes

- Ch. H. Scholz, *The Mechanics of Earthquakes and Faulting* (Cambridge Univ. Press, Cambridge, ed. 2, 2002).
- Working Group on California Earthquake Probabilities, *The Uniform California Earthquake Rupture Forecast, v2, USGS Open File Report 2007* (2008).
- K. E. Sieh, R. H. Jahns, *Geol. Soc. Am. Bull.* **95**, 883 (1984).

- K. E. Sieh, *Bull. Seismol. Soc. Am.* **68**, 1421 (1978).
- G. Schmalzle, T. Dixon, R. Malservisi, R. Govers, *J. Geophys. Res.* **111**, B05403 (2006).
- D. P. Schwartz, K. J. Coppersmith, *J. Geophys. Res.* **89**, 568 (1984).
- J. Liu, Y. Klinger, K. Sieh, C. Rubin, *Geology* **32**, 649 (2004).
- O. Zielke, J. R. Arrowsmith, L. Grant Ludwig, S. O. Akçiz, *Science* **327**, 1119 (2010); published online 21 January 2010 (10.1126/science.1182781).
- G. R. Noriega, thesis, University of California, Irvine (2009).
- L. B. Grant, K. E. Sieh, *Bull. Seismol. Soc. Am.* **83**, 619 (1993).
- L. B. Grant, K. E. Sieh, *J. Geophys. Res.* **99**, 6819 (1994).
- J. Liu-Zeng, Y. Klinger, K. Sieh, C. Rubin, G. Seitz, *J. Geophys. Res.* **111**, B02306 (2006).
- A. Schimmelmann, M. Zhao, C. C. Harvey, C. B. Lange, *Quat. Res.* **49**, 51 (1998).
- A. Schimmelmann, C. B. Lange, B. J. Meggers, *Holocene* **13**, 763 (2003).
- S. O. Akçiz, L. Grant Ludwig, J. R. Arrowsmith, *J. Geophys. Res.* **114**, B01313 (2009).
- W. N. Engstrom, *Quat. Res.* **46**, 141 (1996).
- See supporting material on Science Online.
- D. R. Cayán, K. T. Redmond, L. G. Riddle, *J. Clim.* **12**, 2881 (1999).
- G. R. Noriega, J. R. Arrowsmith, L. B. Grant, J. J. Young, *Bull. Seismol. Soc. Am.* **96**, 33 (2006).
- L. B. Grant, *Science* **272**, 826 (1996).
- S. O. Akçiz *et al.*, *Eos* **87** (fall meet. suppl.), T21E-01 (2006).
- Supported by NSF grants EAR 0409500 and 0711518, USGS grant 07HQGR0092, and the Southern California Earthquake Center (SCEC). SCEC is funded by NSF Cooperative Agreement EAR-0529922 and USGS Cooperative Agreement 07HQAG0008. The SCEC contribution number for this paper is 1305. Thanks to anonymous reviewers, student field assistants, L. Bidart for access to field sites, and J. Southon, M. Kirby, D. Cayán, K. Whipple, A. Heimsath, and E. Vivoni for discussions.

Supporting Online Material

www.sciencemag.org/cgi/content/full/science.1182837/DC1
Materials and Methods
Figs. S1 and S2
References

5 October 2009; accepted 9 January 2010
Published online 21 January 2010;
10.1126/science.1182837
Include this information when citing this paper.

Slip in the 1857 and Earlier Large Earthquakes Along the Carrizo Plain, San Andreas Fault

Olaf Zielke,^{1*} J Ramón Arrowsmith,¹ Lisa Grant Ludwig,² Sinan O. Akçiz²

The moment magnitude (M_w) 7.9 Fort Tejon earthquake of 1857, with a ~350-kilometer-long surface rupture, was the most recent major earthquake along the south-central San Andreas Fault, California. Based on previous measurements of its surface slip distribution, rupture along the ~60-kilometer-long Carrizo segment was thought to control the recurrence of 1857-like earthquakes. New high-resolution topographic data show that the average slip along the Carrizo segment during the 1857 event was 5.3 ± 1.4 meters, eliminating the core assumption for a linkage between Carrizo segment rupture and recurrence of major earthquakes along the south-central San Andreas Fault. Earthquake slip along the Carrizo segment may recur in earthquake clusters with cumulative slip of ~5 meters.

Recent earthquake ruptures along the North Anatolian fault in Turkey [moment magnitude (M_w) 7.4 Izmit earthquake, 1999] (1), the Kunlun Fault in China (M_w 7.8

Kokoxili earthquake, 2001) (2), the Denali fault in Alaska (M_w 7.9 Denali earthquake, 2002) (3), and the Longmenshan fault in China (M_w 7.9 Wenchuan earthquake, 2008) (4) present dramatic

manifestations of large-earthquake phenomena, exemplifying the destructive potential of tectonically active faults. A primary step toward assessing the time and magnitude of future large earthquakes is the identification of earthquake recurrence intervals and along-fault slip-release patterns.

Previous work along the San Andreas Fault (SAF) (5, 6) reported that the largest slip associated with the surface rupture of the M_w 7.9 Fort Tejon earthquake of 1857—the most recent earthquake along the south-central SAF—occurred with ~9 m along the Carrizo segment (Fig. 1). Further investigation along the 1857 rupture trace (7) suggested that individual fault segments experienced essentially the same amount of slip in preceding earthquakes as they did in 1857 (e.g., the largest slip associated with preceding earthquakes occurred with ~9 m along the Carrizo segment). These and similar observations for the Wasatch fault in Utah led to the formulation of the uniform-slip and the characteristic earthquake model (7, 8), which dominate current

seismic hazard assessment and earthquake forecast. Both earthquake recurrence models propose that slip per earthquake at a point along a fault is essentially the same (i.e., characteristic) and can be inferred to have occurred by similar-magnitude major earthquakes. Assuming a constant slip rate along the fault and a direct relation between repeat time and amount of slip released in an earthquake, it was proposed that the relatively strong (i.e., high slip per event) Carrizo segment defines the reported 240- to 450-year recurrence time of major earthquakes along the south-central SAF (7, 9). This widely accepted model is now used to estimate long-term earthquake probabilities along the SAF (10). However, the relation between Carrizo segment rupture and the recurrence of major 1857-like earthquakes, as well as the formulation of the aforementioned earthquake recurrence models, relied on aerial photography and field investigations to reconstruct surface slip of the 1857 earthquake and preceding large earthquakes.

A recently collected light detection and ranging (LIDAR) topographic data set (11) covers the 1857 rupture trace and provides previously unavailable, high-resolution data. LIDAR-based digital elevation models permit identification and measurement of subtle tectono-geomorphic features (12) (Fig. 2A), therefore justifying the re-evaluation of surface slip along the Carrizo segment associated with the 1857 and preceding earthquakes. Here, we present measurements of the lateral surface displacement of well-defined offset stream channels along the Carrizo segment, assuming that channel incision events generally occur more frequently (decadal time scale) than large earthquakes (centennial time scale) (5–7, 9, 13, 14). Consequently, the smallest observable offsets correspond to the most recent earthquake along the Carrizo segment (1857 earthquake), and successive larger offset groups record the cumulative slip of prior events. Channels along the Carrizo segment that show no displacement as they cross the fault trace therefore formed after the 1857 earthquake (5, 6). After fault line and offset stream channels were identified and traced, we determined the position (distance to fault trace) of upstream and downstream topographic, cross-sectional profiles and back-slipped them with respect to one another to determine the channel offset (13) (Fig. 2). Ninety-eight new measurements were combined with 51 remeasured offsets (5) (table S2) along the 60-km-long Carrizo segment (Fig. 1B).

Offset probabilities between 0 and 25 m are spatially well distributed along the fault segment southeast of Wallace Creek (Fig. 3A). The number of offset observations decreases as the respective offset increases, largely due to the steady

degradation of inactive channels by geomorphic processes. The cumulative offset probability distribution (COPD)—stacked offset measurements weighted by assigned quality rating (13)—forms distinct peaks at 5.3, 9.8, 14.9, 20.1, and 24.5 m (Fig. 3B). These peaks, particularly those at 5.3,

9.8, and 14.9 m, are narrow and well separated, indicating that channel offsets along the Carrizo segment fall into small, well-defined ranges. Variation within each offset group appears to be local and random (Fig. 3A). Similar high-frequency and apparently random offset variation has been

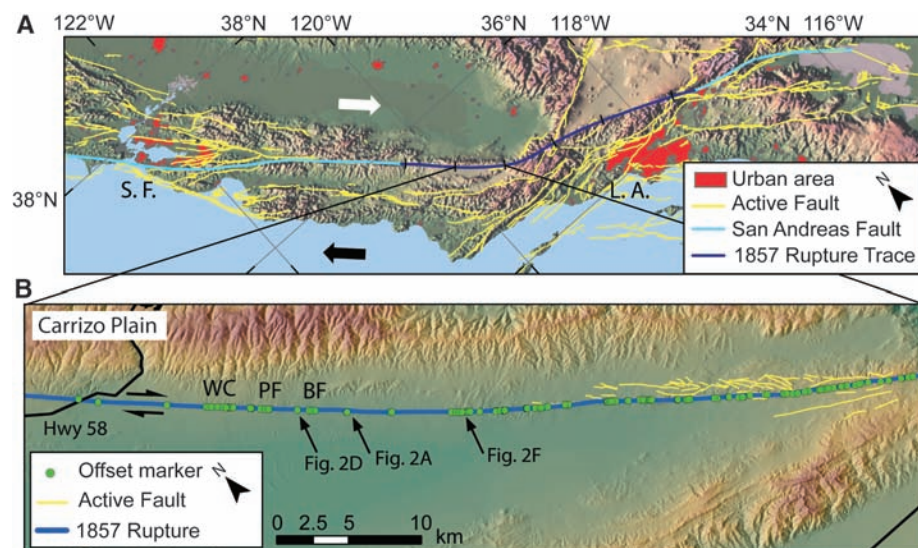


Fig. 1. (A) Overview of Quaternary active faults (27), including the surface rupture of the great 1857 Fort Tejon earthquake along the SAF, and their geographic relation to urban areas (S.F., San Francisco; L.A., Los Angeles). The southern SAF is divided into five major segments (10). Relative motion of North American and Pacific plate is indicated by block arrows. (B) Carrizo Plain segment and the 1857 surface rupture trace. The locations where offset geomorphic markers were measured, as well as selected paleoseismic sites (WC, Wallace Creek; PF, Phelan Fan; BF, Bidart Fan), are indicated.

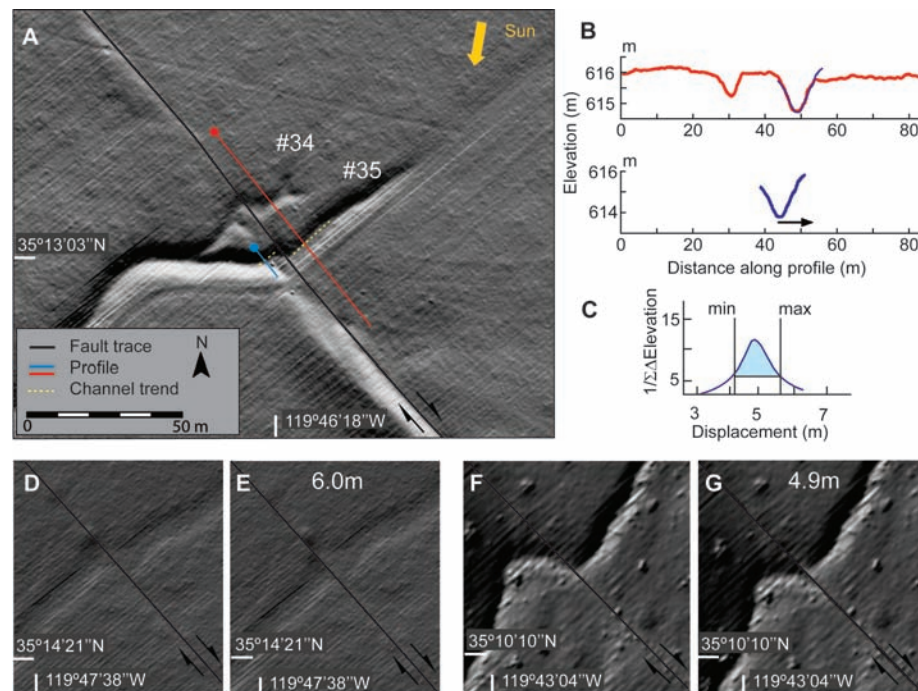


Fig. 2. (A) Hillshade map of channels #34 and #35 (5) generated from LIDAR-based digital elevation models. (B) Topographic profiles along red and blue lines are projected onto the fault plane based on channel obliquity [yellow dashed line in (A)]. Also shown is the blue profile, back-slipped by optimal offset estimate. (C) $1/\Sigma(\Delta\text{elevation})$ is a measure of goodness of fit, calculated for each back-slip increment. (D to G) Current and back-slipped hillshade plot of two channels in the Carrizo Plain area that intersect the SAF and were offset during the 1857 earthquake (Fig. 1B).

¹School of Earth and Space Exploration, Arizona State University, Tempe, AZ 85287, USA. ²Program in Public Health, University of California Irvine, Irvine, CA 92697, USA.

*To whom correspondence should be addressed. E-mail: olaf.zielke@asu.edu

observed for essentially all large historical ruptures—for example, the 1999 Izmit (1) and 2002 Denali earthquakes (3).

The smallest observable offsets are attributed to the 1857 earthquake (Fig. 3). Surface slip distribution and respective COPD peaks reveal that average right-lateral surface displacement of the 1857 rupture along the Carrizo segment was 5.3 ± 1.4 m—distinctly lower than the previously reported 9.0 ± 2.0 m (5–7, 9). We suggest that the latter offsets correspond to the COPD peak at 9.8 m, recording the cumulative slip of two or more earthquakes (15). Prior association of these offsets with the 1857 earthquake is primarily due to the relative geomorphic expression of both channel offset groups. Offset

channels contributing to the COPD peak at 9.8 m form a stronger geomorphic signal (relatively deeply incised, wide channels) than the presumably younger but locally only weakly developed channels that were offset by 5.3 ± 1.4 m; spatiotemporal variations in storm severity are likely the controlling factor (16–18). As a result, earlier studies using aerial photography and field observations to measure the 1857 surface slip distribution may have missed those often weakly developed 5.3 ± 1.4 m offsets or interpreted them as outliers not representative of the 1857 surface slip (5–7). Paleoseismic studies at Phelan Fan and Wallace Creek (Fig. 1B) determined minimum channel offsets of 6.7 and 7.9 m, respectively (9, 14), associating them with the 1857

earthquake. Their observations were of uniquely matching and singly incised offset channel margins and fill units. Whereas the former offset lies marginally in the observed range for the 1857 event, the latter offset does not. The discrepancy between the Wallace Creek record [reporting a cumulative slip of 7.9, 15.8, 20.7, 22.0, and 30.0 m (9)] and our COPD peaks (Fig. 3B) may be related to along-fault slip variations or spatiotemporal variations in relative frequency of channel incision and earthquake occurrence. A recent study on modern earthquakes (19) showed that the ratio between average and maximum surface slip is ~ 0.4 . Considering a ~ 5 -m average slip during the 1857 event in the Carrizo Plain, the observed 7.9 m at Wallace Creek may reflect the maximum slip of this event. However, it was noted (9) that channel offsets may record the cumulative slip of multiple events when earthquake recurrence was more frequent than channel formation. We suggest that the 7.9-m offset channel formed before the penultimate earthquake and therefore records the slip of more than one earthquake (15).

Estimates of seismic moment (M_0) and M_w for the 1857 earthquake change by only a fraction if the new offsets for the Carrizo segment are used; the respective values change from $M_0 \sim 8.71 \times 10^{20}$ Nm to $M_0 \sim 8.12 \times 10^{20}$ Nm and from M_w 7.93 to M_w 7.90 (table S3). The new combined surface slip distribution for the 1857 earthquake (Fig. 4) suggests that the Carrizo segment may not be considered an individual fault segment because its respective offset is not distinctly different from that of the neighboring segments (Fig. 1A). Neither distinctively large slip along the Carrizo segment (relative to other sections of the 1857 rupture) nor high slip gradients at its proposed boundaries (5, 7) were observed. These observations challenge the long-held view that the Carrizo segment is an unusually strong fault segment, responsible for the recurrence of major 1857-like earthquakes along the south-central SAF (7–10). The 1857 multisegment rupture may not be the typical (i.e., characteristic) earthquake for the south-central SAF. The Carrizo Plain and other fault sections involved in the great 1857 earthquake may therefore rupture individually and in smaller but still hazardous events; major, 1857-like rupture may occur only infrequently.

Previous work along the SAF system described bimodality in the magnitude-frequency distribution (20–22); small- to moderate-magnitude earthquakes follow the Gutenberg-Richter inverse power-law relation, whereas large-size earthquakes occur more frequently. According to earthquake simulations (23), bimodality may be explained by systematic variations of coseismic stress drop with depth and a resulting abrupt increase in down-dip rupture width at the transition from moderate- to large-magnitude earthquakes. Total strain release along faults is presumably dominated by large-earthquake slip (7, 8, 20–23). If

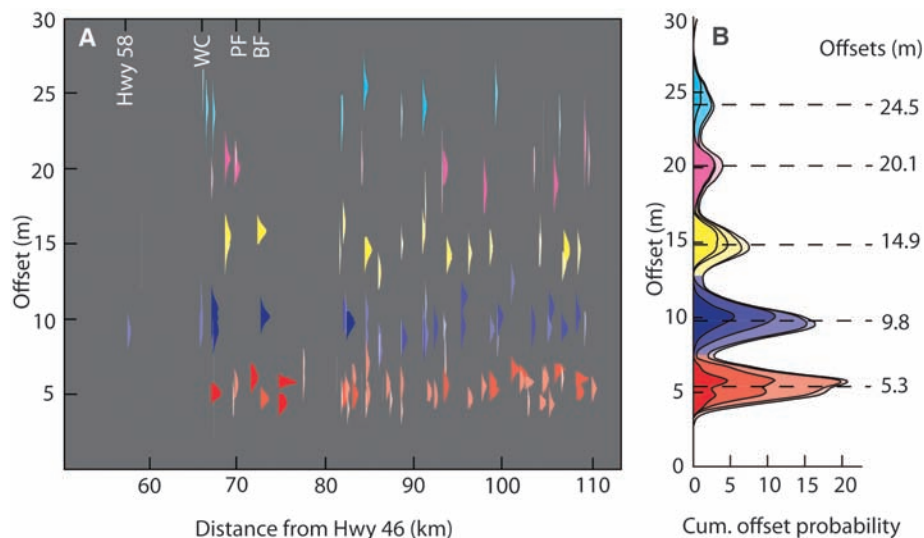


Fig. 3. (A) Offset probability for individual measurements along the Carrizo segment. The goodness-of-fit measurements were truncated by visually determining minimum and maximum offsets for each offset (13). Color is assigned based on the respective optimal offset measurement (red: 5 ± 2.5 m; blue: 10 ± 2.5 m; yellow: 15 ± 2.5 m; magenta: 20 ± 2.5 m; and cyan: 25 ± 2.5 m), indicating to which COPD peak it contributes most. Color intensity is based on the quality rating assigned to the measurement. (B) COPD color intensity is based on the quality rating of the offset estimates used in the stacking. The COPD forms narrow, well-separated peaks.

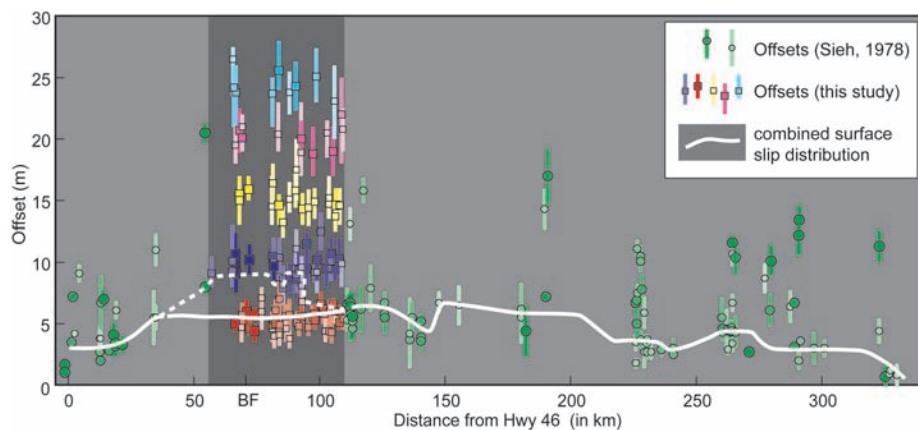


Fig. 4. Combined surface slip distribution associated with the 1857 earthquake (solid white line). Measurements show quality rating increasing with increasing color intensity. Our measurements along the Carrizo Plain suggest an average slip of 5.3 ± 1.4 m during this event. The previously reported 9.0 ± 2.0 m offsets (dashed white line) represent the cumulative slip of at least two earthquakes.

bimodal behavior is a property of SAF earthquake recurrence, the observed COPD peaks at 5.3, 9.8, 14.9, 20.1, and 24.5 m (Fig. 3B) represent the cumulative slip of the five most recent clusters of earthquakes, each consisting of a single large earthquake and an undefined number of small- to moderate-size earthquakes (15). Recent work at the Bidart Fan site (18) on the Carrizo Plain (Fig. 1B) provides support for clusters of earthquakes that add up to 5-m slip. An alternative interpretation is that slip varies from event to event unsystematically and that the observed COPD peaks (Fig. 3B) are caused by infrequent but highly episodic channel incision events, recording the earthquake slip that was accumulated along the fault in between incision events. Then channel incision—not earthquake slip—has a characteristic recurrence pattern (16). Assuming that total strain release along the Carrizo segment is dominated by large-earthquake slip (7, 8, 21–23) and considering the Holocene slip rate of 35 mm/year along the SAF in the Carrizo Plain (7), we estimate a 140 ± 46 year interval for large-earthquake recurrence (24). This recurrence time is consistent with findings of past paleoseismic studies in the Carrizo Plain (25, 26), which may have recognized primarily large earthquakes with compelling rupture evidence. Surface-rupturing earthquakes along the Carrizo segment therefore occur more frequently and with lower (but still high) slip than previously reported (5–7, 9, 14, 26).

References and Notes

1. T. Rockwell *et al.*, *Bull. Seismol. Soc. Am.* **92**, 79 (2002).
2. A. Lin *et al.*, *Science* **296**, 2015 (2002).
3. P. J. Haeussler *et al.*, *Bull. Seismol. Soc. Am.* **94** (6B), S23 (2004).
4. X. W. Xu *et al.*, *Geology* **37**, 515 (2009).
5. K. E. Sieh, *Bull. Seismol. Soc. Am.* **68**, 1421 (1978).
6. R. E. Wallace, in *Proceedings of Conference on Geologic Problems of the San Andreas Fault System*, W. R. Dickinson, A. Grantz, Eds. (Stanford Univ. Publications in the Geological Sciences, 1968), vol. 11, p. 6.
7. K. E. Sieh, R. H. Jahns, *Geol. Soc. Am. Bull.* **95**, 883 (1984).
8. D. P. Schwartz, K. J. Coppersmith, *J. Geophys. Res.* **89**, (B7), 5681 (1984).
9. J. Liu-Zeng, Y. Klinger, K. Sieh, C. Rubin, G. Seitz, *J. Geophys. Res.* **111** (B2), B02306 (2006).
10. 2007 Working Group of California Earthquake Probabilities, *The Uniform California Earthquake Rupture Forecast, Version 2 (UCERF 2)* (USGS Open File Report 2007-1437, 2008; <http://pubs.usgs.gov/of/2007/1437/>).
11. LiDAR data freely available at www.opentopography.org/.
12. J. R. Arrowsmith, O. Zielke, *Geomorphology* **113**, 70 (2009).
13. Materials and Methods are available as supporting material on Science Online.
14. L. B. Grant, K. E. Sieh, *Bull. Seismol. Soc. Am.* **83**, 619 (1993).
15. The number of earthquakes contributing to individual COPD peaks (Fig. 3B) is a priori not known. Cumulative offset from two or more events might be misinterpreted as single-event offset because short interevent time and temporal variations in storm severity (16–18) may suppress channel incision between successive events, so that no or only weak evidence for the latter event might be created.
16. A. Schimmelmann, C. B. Lange, B. J. Meggers, *Holocene* **13**, 763 (2003).
17. M. A. Cane, S. E. Zebiak, *Science* **228**, 1085 (1985).
18. L. Grant Ludwig, S. O. Akçiz, G. R. Noriega, O. Zielke, J. R. Arrowsmith, *Science* **327**, 1117 (2010); published online 21 January 2010 (10.1126/science.1182837).
19. S. G. Wesnousky, *Bull. Seismol. Soc. Am.* **98**, 1609 (2008).
20. L. Knopoff, *Proc. Natl. Acad. Sci. U.S.A.* **97**, 11880 (2000).
21. S. G. Wesnousky, *Bull. Seismol. Soc. Am.* **84**, 1940 (1994).
22. J. Ben-Zion, *Rev. Geophys.* **46**, RG4006 (2008).
23. O. Zielke, J. R. Arrowsmith, *Geophys. Res. Lett.* **35**, L24301 (2008).
24. The 140 ± 46 year interval presents a maximum for the recurrence of major earthquakes along the Carrizo segment because it neglects the potential slip contribution of moderate-size earthquakes.
25. S. O. Akçiz, L. Grant Ludwig, J. R. Arrowsmith, *J. Geophys. Res.* **114**, B01313 (2009).
26. L. Grant, K. E. Sieh, *J. Geophys. Res.* **99**, 6819 (1994).
27. U.S. Geological Survey and California Geological Survey, *Quaternary Fault and Fold Database of the United States* (<http://earthquake.usgs.gov/regional/qfaults/>).
28. This research was supported by the NSF Tectonics Program and the Southern California Earthquake Center (SCEC). SCEC is funded by NSF Cooperative Agreement EAR-0529922 and U.S. Geological Survey Cooperative Agreement 07HQAG0008. The SCEC contribution number for this paper is 1310. We thank T. Jordan, D. Schwartz, and anonymous reviewers for constructive comments.

Supporting Online Material

www.sciencemag.org/cgi/content/full/science.1182781/DC1
Materials and Methods
Figs. S1 to S4
Tables S1 to S3
References

2 October 2009; accepted 5 January 2010
Published online 21 January 2010;
10.1126/science.1182781
Include this information when citing this paper.

Plant Peptides Govern Terminal Differentiation of Bacteria in Symbiosis

Willem Van de Velde,¹ Grigor Zehirov,² Agnes Szatmari,^{1,3} Monika Debreczeny,⁴ Hironobu Ishihara,² Zoltan Kevei,⁴ Attila Farkas,⁴ Kata Mikulass,⁴ Andrea Nagy,⁴ Hilda Tiricz,⁴ Beatrice Satiat-Jeunemaître,¹ Benoit Alunni,¹ Mickael Bourge,¹ Ken-ichi Kucho,² Mikiko Abe,² Attila Kereszt,⁴ Gergely Maroti,⁴ Toshiki Uchiumi,² Eva Kondorosi,^{1,4*} Peter Mergaert¹

Legume plants host nitrogen-fixing endosymbiotic *Rhizobium* bacteria in root nodules. In *Medicago truncatula*, the bacteria undergo an irreversible (terminal) differentiation mediated by hitherto unidentified plant factors. We demonstrated that these factors are nodule-specific cysteine-rich (NCR) peptides that are targeted to the bacteria and enter the bacterial membrane and cytosol. Obstruction of NCR transport in the *dnf1-1* signal peptidase mutant correlated with the absence of terminal bacterial differentiation. On the contrary, ectopic expression of NCRs in legumes devoid of NCRs or challenge of cultured rhizobia with peptides provoked symptoms of terminal differentiation. Because NCRs resemble antimicrobial peptides, our findings reveal a previously unknown innovation of the host plant, which adopts effectors of the innate immune system for symbiosis to manipulate the cell fate of endosymbiotic bacteria.

Symbiotic nitrogen fixation by legumes is a major contributor to the combined nitrogen pool in the biosphere. It takes place in specialized root organs called nodules (1). The symbiotic nodule cells are large polyploid cells (2) housing thousands of bacteroids. Bacteroids are differentiated *Rhizobium* bacteria with specialized metabolic activity, capable of reducing atmospheric nitrogen and supplying the

plant with ammonium as a nitrogen source (3). In addition to this metabolic adaptation, the endosymbionts of *Medicago truncatula* and related legumes undergo striking morphological changes such as cell elongation coupled to genome amplification, membrane modifications, and the loss of reproductive capacity (4–6). The polyploid state of bacteroids and the induction of bacteroid-like cells by genetic interference

with the rhizobial cell cycle (7–10) suggest that terminal bacteroid differentiation is a cell cycle-related process.

This terminal bacteroid differentiation is specific for legumes belonging to the inverted repeat-lacking clade (IRLC) such as *Medicago*, *Pisum*, or *Trifolium*, whereas bacteroids in the non-IRLC legumes, such as *Lotus japonicus*, show no sign of terminal differentiation as they maintain their normal bacterial size, genome content, and reproductive capacity (6). The same *Rhizobium* strains that form symbiosis with both IRLC and non-IRLC legumes have different bacteroid differentiation fates in the two legume types. Therefore, it was concluded that terminal bacteroid differentiation is determined by unknown host factors that are produced by the IRLC legumes and do not exist in the non-IRLC legumes (6). The nodule-specific cysteine-rich (NCR) peptides were likely candidates for these factors (11, 12). NCR genes were found only in

¹Institut des Sciences du Végétal, Centre National de la Recherche Scientifique, 91198 Gif-sur-Yvette Cedex, France.

²Graduate School of Science and Engineering, Kagoshima University, 890 0065 Kagoshima, Japan. ³Plant Protection Institute of the Hungarian Academy of Sciences, 1022 Budapest, Hungary. ⁴Institute for Plant Genomics, Human Biotechnology and Bioenergy, Bay Zoltan Foundation for Applied Research, 6726 Szeged, Hungary.

*To whom correspondence should be addressed. E-mail: eva.kondorosi@isv.cnrs-gif.fr